Evidence for diffractive charm production in ν_μFe and $\bar{\nu}_\mu$Fe scattering at the Fermilab Tevatron

T. Adams, A. Alton, T. Bolton, J. Goldman, M. Goncharov, and D. Naples*
Kansas State University, Manhattan, Kansas 66506

R. A. Johnson, M. Vakili,† and V. Wu
University of Cincinnati, Cincinnati, Ohio 45221

J. Conrad, B. T. Fleming, J. Formaggio, S. Koutsoliotas,‡ J. H. Kim,§ C. McNulty, A. Romosan,‖ M. H. Shaevitz, P. Spentzouris,¶ E. G. Stern, A. Vaitaitis, and E. D. Zimmerman
Columbia University, New York, New York 10027

R. H. Bernstein, L. Bugel, M. J. Lamm, W. Marsh, P. Nienaber,** and J. Yu
Fermi National Accelerator Laboratory, Batavia, Illinois 60510

L. de Barbaro, D. Buchholz, H. Schellman, and G. P. Zeller
Northwestern University, Evanston, Illinois 60208

J. Brau, R. B. Drucker, R. Frey, and D. Mason
University of Oregon, Eugene, Oregon 97403

S. Avvakumov, P. de Barbaro, A. Bodek, H. Budd, D. A. Harris,¶ K. S. McFarland, W. K. Sakumoto, and U. K. Yang
University of Rochester, Rochester, New York 14627

(Received 24 September 1999; published 14 March 2000)

We present evidence for the diffractive processes $\nu_\mu\mathrm{Fe}\to\mu^- D_S^+(D_S^*)\mathrm{Fe}$ and $\bar{\nu}_\mu\mathrm{Fe}\to\mu^+ D_S^-(D_S^*)\mathrm{Fe}$ using the Fermilab SSQT neutrino beam and the Lab E neutrino detector. The data are consistent with standard model production of the neutrino trident reactions $\nu_\mu\mathrm{Fe}\to\nu_\mu\mu^-\mu^+\mathrm{Fe}$ and $\bar{\nu}_\mu\mathrm{Fe}\to\bar{\nu}_\mu\mu^+\mu^-\mathrm{Fe}$. We see no evidence for neutral-current production of J/ψ via either diffractive or deep inelastic scattering mechanisms.

PACS number(s): 13.15+g, 12.15.−y, 12.40.Vv, 13.60.Le

I. INTRODUCTION

Opposite-signed two-muon production in deep inelastic scattering (DIS) with neutrinos or anti-neutrinos serves as a reliable signal for charm quark production through the sequence

$$\nu_\mu N\to\mu^- DX,\quad D\to\mu^+\nu_\mu X',\tag{1.1}$$

where D represents a weakly decaying charmed hadron. This is especially true in dense targets such as the NuTeV detector at Fermilab where absorption of pions and kaons in the hadronic shower suppresses backgrounds from meson decay that occur via

$$\nu_\mu N\to\mu^-\pi^+(K^+)X,\quad \pi^+(K^+)\to\mu^+\nu_\mu.\tag{1.2}$$

Previous studies of DIS two-muon production in neutrino interactions [1–6] have yielded important measurements of the Cabibbo-Kobayashi-Maskawa (CKM) matrix elements V_{cd} and V_{cs}, the effective charm quark mass, and the size and shape of the nucleon strange sea. These studies were performed in the context of the QCD-corrected quark-parton model and hence were restricted to large values of energy transfer, ν, to the struck nucleon, resulting in large amounts of observed hadronic energy, E_{HAD}.

At low hadronic energy, one expects to observe charm production via another mechanism, namely, diffractive production of pseudoscalar and vector D_S mesons via both coherent and incoherent scattering:

$$\nu_\mu A\to\mu^- D_S^+ A,\quad \nu_\mu A\to\mu^- D_S^+\gamma_{\mathrm{SOFT}}A,\tag{1.3}$$

where the low energy decay photon γ_{SOFT} will accompany the production of vector D_S^*, $A=\mathrm{Fe}$, for coherent production in our experiment, and $A=n$ or p for incoherent production. Here, large energy transfer to the meson may not result in large hadronic energy because the nucleus remains intact.

These reactions have been observed at the few event level in bubble chamber and emulsion experiments [7,8]. It is important to understand the size of this diffractive contribution because of its influence as a background to DIS charm production. These processes are also of interest to future high

*Present address: University of Pittsburgh, Pittsburgh, PA 15260.
†Present address: Texas A&M University, College Station, TX 77843.
‡Present address: Bucknell University, Lewisburg, PA 17837.
§Present address: University of California, Irvine, CA 92697.
‖Present address: University of California, Berkeley, CA 94720.
¶Present address: Fermi National Laboratory, Batavia, IL 60510.
**Present address: Marquette University, Milwaukee, WI 53201.

statistics neutrino experiments at a muon collider. They provide the possibility of measuring the ratio V_{cd}/V_{cs} via comparison of the rates $\nu_\mu A \to \mu^- D^{*+} A$ and $\nu_\mu A \to \mu^- D_S^{*+} A$. Additionally, they can create a signature which mimics quasi-elastic production of τ leptons through the chain $\nu_\mu A \to \mu^- D_S^+ (\gamma_{\rm SOFT}) A$, $D_S^+ \to \tau^+ \nu_\tau$, which may be of concern to high sensitivity $\nu_\mu \to \nu_\tau$ oscillation searches.

A competing reaction that produces the same experimental signature, an opposite-signed muon pair with vanishing E_{HAD}, is the neutrino trident process [9,10]

$$\nu_\mu A \to \mu^- \mu^+ \nu_\mu A. \tag{1.4}$$

In principle, the neutrino trident reaction provides an interesting test of electroweak theory since contributions from W and Z decay produce a reliably calculable 40% destructive interference effect. In practice, the very small cross section implies that only a handful of neutrino tridents have previously been observed in neutrino scattering. Furthermore, the neutrino trident process must be considered in combination with the expected signal from diffractive charm production in experiments that are only sensitive to two-muon final states. This point has not been recognized in previous measurements of neutrino tridents.

NuTeV (Fermilab Experiment E815) is a high-statistics experiment studying neutrino and anti-neutrino interactions with a high intensity, high energy sign-selected beam. Its primary goal is to measure the electroweak mixing angle $\sin^2\theta_W$; however, the high-statistics nature makes it possible to study the rarer processes described above. At low (zero) hadronic energy the dominant DIS processes fall off and additional channels such as diffractive $D_S^\pm / D_S^{*\pm}$ production [8], neutrino trident [9,10], and diffractive J/ψ [11] become more important. This is the first analysis to study the inclusive production of all processes in the final state with low hadronic energy and two muons.

The next section will describe the NuTeV experiment while Sec. III details the data selection. Predictions for the sources of low-E_{HAD} two muon events are given in Sec. IV. Section V details the charged- and neutral-current analyses and conclusions are stated in the final section.

II. NuTeV EXPERIMENT

The NuTeV experiment ran at Fermilab using the refurbished Lab E detector [12] and ν_μ and $\overline{\nu_\mu}$ beams provided by the newly installed Sign-Selected Quadrupole Train (SSQT) [13]. The SSQT has the capability of selecting either muon neutrino or muon anti-neutrino beams while leaving $\lesssim 2\times 10^{-3}$ of the anti-selected type.

The Lab E detector, located 1.5 km downstream of the primary target, consists of a target calorimeter followed by a toroid spectrometer (Fig. 1). The calorimeter is composed of 42 segments of four steel plates, two liquid scintillator counters (SCs) and one drift chamber (DC) (Fig. 2). The steel provides mass for the neutrino target, the SCs measure the longitudinal vertex and energy deposition (E), and the DC is used to find the transverse vertex and reconstruct downstream tracks. Because of the high density of the target, only muons deeply penetrate the calorimeter, and all other particles create a hadronic or electromagnetic shower near the interaction vertex.

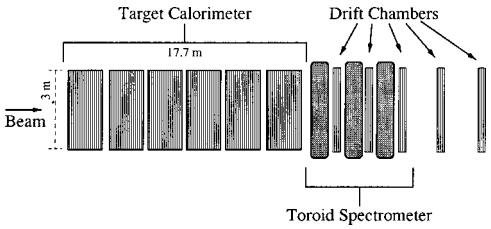

FIG. 1. Schematic drawing of the Lab E detector. Beam enters from the left. The target calorimeter is on the left and the toroid spectrometer is on the right.

The toroid spectrometer, located immediately downstream of the calorimeter, focuses muons from the primary charged-current vertex given the type of beam (ν_μ or $\overline{\nu_\mu}$), measuring both charge and momentum (p) of muons with $p \geqslant 5$ GeV/c which enter the spectrometer. It is also possible to measure the momentum of a subset of muons with $5 \leqslant p \leqslant 15$ GeV/c which range out in the calorimeter and to place a lower bound on the momentum of muons which exit the side of the calorimeter.

The NuTeV detector was calibrated with a separate beam of hadrons, muons, or electrons throughout the running period of the experiment. Hadronic and muon energy scales for the calorimeter were determined to 0.43% and 1.0% respectively over the energy range 5–200 GeV [14]. Muon momentum measurement in the spectrometer is limited by multiple Coulomb scattering to $\Delta p/p = 0.11$, and the sampling-dominated hadronic resolution was approximately $\Delta E/E = 0.86/\sqrt{E}$.

III. EVENT SELECTION

Analyses presented here use the full NuTeV data sample from the 1996–1997 fixed-target run corresponding to 1.3×10^{18} protons on target (POT) for neutrino running and 1.6×10^{18} protons on target for anti-neutrino running. The sizes of various event samples from NuTeV are listed in Table I.

Events were selected for the low-E_{HAD} two-muon analysis based on the following criteria:

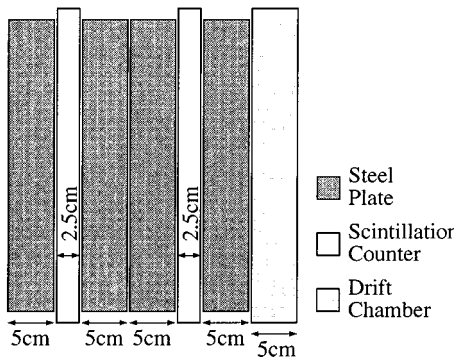

FIG. 2. Drawing of one segment of the Lab E calorimeter.

TABLE I. NuTeV event samples.

	No. of events (ν)	No. of events ($\bar{\nu}$)
Single muon (all E_{HAD})	1.3×10^6	0.46×10^6
Two muons (all E_{HAD})	4300	1300
Single muon ($E_{HAD}<3$ GeV)	0.10×10^6	0.06×10^6
Two muons ($E_{HAD}<3$ GeV)	33	21

(i) The event vertex was required to be at least 25 cm from any side, 40 cm steel equivalent from the upstream end and 1.4 m steel equivalent from the downstream end of the calorimeter.

(ii) At least two muons were required to be found and fitted by the tracking code. At least one of these had to be reconstructed in the toroid spectrometer with a momentum greater than 9 GeV/c.

(iii) The second muon's momentum could be obtained by either toroid spectrometer or range information; its momentum was required to be at least 5 GeV/c.

(iv) Either the calorimeter drift chamber or scintillator counter signals had to be consistent with passage of two muons over five drift chambers or seven scintillator counters starting at the event vertex.

(v) The hadronic energy is determined by summing the energy in the scintillator counters from the upstream end of the shower to 5 counters past the downstream end of the shower. The upstream end of the shower is defined as the first of two consecutive counters with more than 1/4 of the energy deposited by minimum-ionizing particles (MIPs). The downstream end of the shower is defined as the counter before the first place where three consecutive counters have energy less than 3 MIPs. Also, for events with reconstructed muons a parametrized dE/dx for each muon is subtracted from the measured energy.

IV. LOW HADRONIC ENERGY: TWO MUON SOURCES

The analysis strategy consists of comparing data to a model comprised of all known sources of events with two muons and small hadronic energy. Kinematic distributions were generated according to electroweak theory for neutrino trident production, leading order quark-parton model predictions for DIS feed-down, and vector meson dominance (VMD) or partially conserved axial vector current (PCAC) models extended to four flavors for diffractive charm production. Detector response was modeled using a GEANT-based Monte Carlo program (GEANT 3.21), with simulated events processed in an identical fashion as data. The following sections describe the various sources and predictions for their rates.

A. DIS charm production

Neutrino DIS produces two major sources of two-muon events. Charged-current charm production can result in a second muon from the decay of the charmed meson [Fig. 3(a)]. Also, during charged-current interactions, a π/K in the hadronic shower can decay to a muon and a neutrino before interacting [Fig. 3(b)].

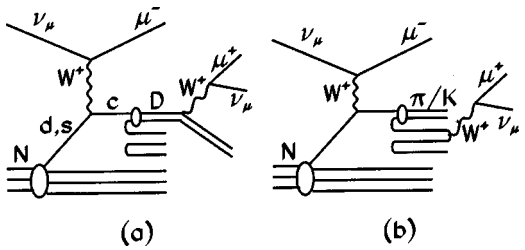

FIG. 3. The Feynman diagrams for DIS production of two-muon events: (a) DIS charged-current production of charm with a semimuonic decay, (b) DIS charged-current production with a π/K decay in the hadronic shower.

Two-muon events from DIS charm were modeled via leading order predictions using d and s parton distribution functions measured in this and previous experiments [2–6] assuming an effective charm quark mass $m_c=1.32$ GeV/c^2. Charm quark fragmentation was treated using the Collins-Spiller scheme [15] with fragmentation parameter $\epsilon=0.93$ and $D^0{:}D^+{:}\Lambda_C^+$ production ratios as measured in Fermilab E531 [16], corrected for effects of D_S^+ production [17]. Charmed hadron decay was modeled using the best available data as summarized by the Particle Data Group [18], with particular attention given to purely leptonic decays.

Two muon events from π/K decay in the hadron showers of ordinary charged-current (CC) events were modeled using measured parametrizations [19] from a previous experiment (Fermilab E744/770) which ran at similar neutrino energies and used the same neutrino target.

The hadronic energy (E_{HAD}) spectrum for DIS two-muon Monte Carlo events is shown in Fig. 4. While these sources generally contain significant amounts of hadronic energy, some contribution at low E_{HAD} is seen. Normalizing to the high-E_{HAD} ($E_{HAD}>5$ GeV) two-muon sample we predict 10.4 (4.0) events with $E_{HAD}<3$ GeV in the ν ($\bar{\nu}$) mode due to the low hadronic energy tail of the DIS process.

B. Neutrino tridents

Neutrino trident production is a purely electroweak process in which interference between the charged- and neutral-

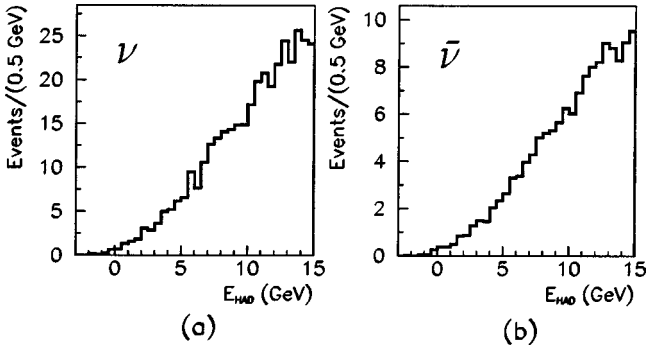

FIG. 4. Distribution of expected hadronic energy (E_{HAD}) for DIS production of two-muon events (Monte Carlo simulation). This analysis is concerned with the contribution near zero.

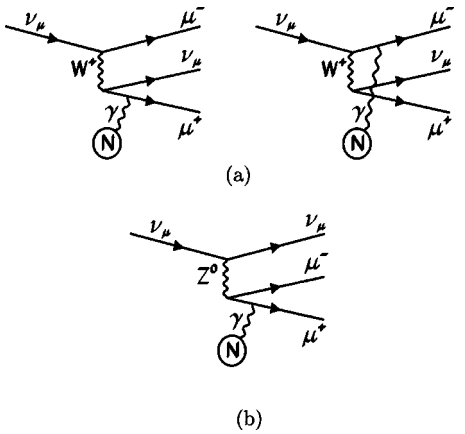

FIG. 5. The Feynman diagrams for neutrino trident production: (a) charged-current production; (b) neutral-current production.

current diagrams causes a 40% decrease (from $V-A$) in the total cross section [9,10,20]. Feynman diagrams are shown in Fig. 5. The small ($\sim 10^{-4}$ fb/nucleon) cross section has limited the observation until recent years [21–23].

For this analysis, the Monte Carlo simulation was generated using the full matrix element with W-Z interference [24,25] including contributions from both coherent nuclear and incoherent nucleon scattering. This procedure incorporated all possible kinematic correlations between the two muons and represents an improvement over previous methods [21,26]. In particular, there is a strong correlation between the energies of the two muons which is very important to the acceptance: when one muon's momentum is high, the other's is preferentially very low.

The lengthy expression for the cross section can be found in Refs. [9,10,20,24,25]. The rate depends on the electroweak mixing angle, which we set to $\sin^2\theta_W = 0.2222$, and, weakly, on nuclear and nucleon form factors. Standard dipole parametrizations were used for the latter with a vector pole mass $m_V^2 = 0.71\ \mathrm{GeV}^2/c^4$. The nuclear form factor for iron was calculated assuming a Fermi charge density function for iron with nuclear size parameter $c = 3.9$ fm and thickness parameter $b = 0.55$ fm.

NuTeV should observe 4.8 (2.2) neutrino trident events in the ν ($\bar{\nu}$) mode from both coherent and incoherent production.

C. $D_S^{\pm}/D_S^{*\pm}$ production

Diffractive production of $D_S^{\pm}(D_S^{*\pm})$ (Fig. 6) has been observed in previous experiments [7,8] and contributes to the

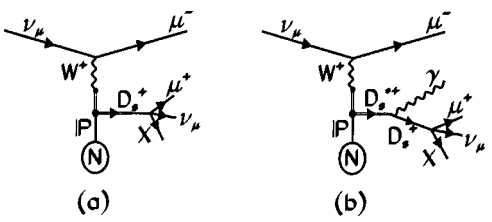

FIG. 6. The Feynman diagrams for (a) $D_S^{\pm}$ and (b) $D_S^{*\pm}$ production.

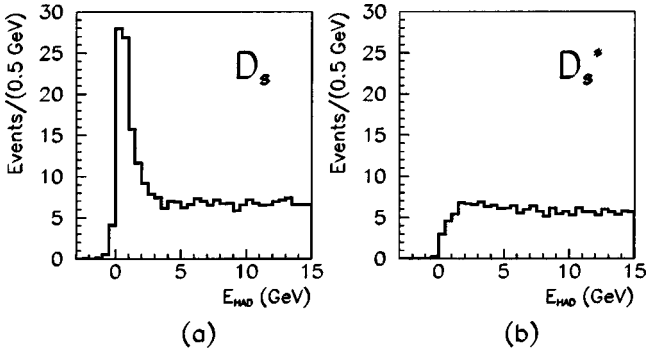

FIG. 7. The E_{HAD} distributions for (a) $D_S^{\pm}$ and (b) $D_S^{*\pm}$ Monte Carlo simulation.

low-E_{HAD} two-muon sample whenever the D_S meson decays either to all-lepton final states ($D_S^+ \to \tau^+\nu_\tau, \tau^+ \to \mu^+\nu_\mu\bar{\nu}_\tau$ or $D_S^+ \to \mu^+\nu_\mu$) or to final states with small hadronic energy ($D_S^+ \to \mu^+\nu_\mu X_{\mathrm{SOFT}}$). The latter case was modeled by assuming that the D_S^+ semi-muonic decay rate was saturated by the channels $D_S^+ \to \phi\mu^+\nu_\mu$, $\eta\mu^+\nu_\mu$, $\eta'\mu^+\nu_\mu$ in the measured proportions summarized by the Particle Data Group [18]. Only contributions from coherent diffractive production were considered. Incoherent production of $D_S^+(D_S^{*\pm})$ from νN scattering is already included in the inclusive DIS rate.

Vector D_S^* production was modeled assuming a VMD type mechanism with cross section given by

$$\frac{d^3\sigma(\nu_\mu N \to \mu D_S^* N)}{dQ^2 d\nu dt} = \frac{Q^2\nu}{g_\rho^2 E^2}\frac{M_{D_S^*}^2}{(Q^2+M_{D_S^*}^2)^2}\frac{1}{(1-\epsilon)}A^\beta\frac{e^{-bt}}{b}, \tag{4.1}$$

where Q^2 and ν are the momentum and energy transfer to the D_S^*, t is the square of the momentum transfer to the nucleus, g_ρ is the ρ coupling constant, $M_{D_S^*}$ is the mass of the D_S^* meson, E is the incoming neutrino energy, ϵ is virtual W polarization ($\epsilon = [4E(E-\nu)-Q^2]/[4E(E-\nu)+Q^2+2\nu^2]$), A is the atomic number of the target nucleus, β determines the A dependence [$\beta = (3{*}Q^2+2)/(3{*}Q^2+3)$ incoherent, $\beta = 2$ coherent] and b is the slope of the distribution of momentum transfer squared (t) to the nucleus (nucleon) ($b = 3$ incoherent, $b = 145$ coherent). A check was performed which showed that the NuTeV experiment is in-

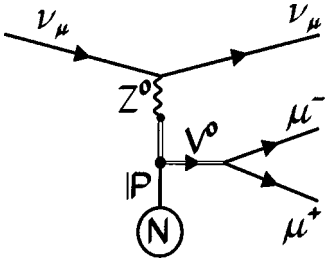

FIG. 8. The Feynman diagram for neutral-current diffractive production of light vector mesons (V^0). Here V^0 can be a ρ^0, ω, ϕ, or J/ψ meson and N represents either a nucleus (coherent) or nucleon (incoherent).

TABLE II. VMD predictions for the expected number of diffractively produced light vector mesons which decay to two muons.

	No. of events (coherent) (ν)	No. of events (incoherent) (ν)	No. of events (coherent) ($\bar{\nu}$)	No. of events (incoherent) ($\bar{\nu}$)
ρ^0	0.0074	0.0039	0.0037	0.0019
ω	0.023	0.016	0.011	0.008
ϕ	0.036	0.022	0.018	0.011
J/ψ	4.88	17.1	1.86	7.76

sensitive to effects of the virtual-W polarization on the D_S^* decay. The overall normalization was left to be determined by the data. To set the scale, the normalization was also obtained in the $SU(4)$-flavor limit by comparing to the measured cross section for diffractive ρ^+ production in neutrino scattering.

The number of events expected by NuTeV is normalized to the observed two-muon data with $E_{HAD}>5$ GeV:

$$N_M=\frac{\int \Phi(E_\nu)\sigma_M(E_\nu)\epsilon(E_\nu)B_M dE_\nu}{\int \Phi(E_\nu)\sigma_{\mu\mu}(E_\nu)\epsilon(E_\nu)B_{\mu\mu}dE_\nu}N_{\mu\mu}, \quad (4.2)$$

where M refers to the meson being produced, $\mu\mu$ refers to DIS two-muon data, Φ is the NuTeV flux, σ is the cross section, E_ν is the incident neutrino energy, ϵ is the detection efficiency, B is the (semi-)muonic branching fraction, and $N_{\mu\mu}$ is the number of DIS two-muon events observed in the NuTeV data. Throughout this analysis, we normalize the predicted number of events to the high-E_{HAD} two muon data which have been studied elsewhere [2]. This procedure predicts 33.0 (13.6) observed D_S^* events for ν ($\bar{\nu}$) mode in NuTeV.

The contribution of pseudoscalar D_S^+ decay was estimated using PCAC formulas [27,28] adapted for charm:

$$\frac{d^3\sigma(\nu_\mu N\to\mu D_S N)}{dQ^2 d\nu dt}=\frac{\nu}{E^2}\frac{\epsilon}{(1-\epsilon)}\frac{M_{D_{S1}}^4}{(Q^2+M_{D_{S1}}^2)^2}f_{D_S}^2 A^\beta \frac{e^{-bt}}{b}, \quad (4.3)$$

where $M_{D_{S1}}$ is the mass of the D_{S1} meson, f_{D_S} is the D_S decay constant ($f_{D_S}=0.31$ GeV), and b is the slope of the distribution of momentum transfer squared (t) to the nucleus

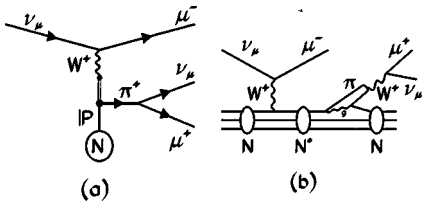

FIG. 9. The Feynman diagrams for single $\pi^\pm$ production: (a) diffractive and (b) resonance.

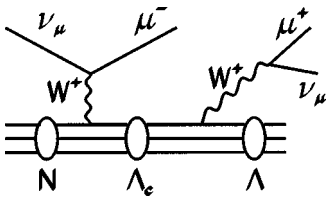

FIG. 10. The Feynman diagram for diffractive $\Lambda_C^\pm$ production.

(nucleon) ($b=3$ incoherent, $b=60$ coherent). Here 102.9 (48.2) events are predicted for ν ($\bar{\nu}$) mode in the SU(4) flavor limit.

Figure 7 shows the E_{HAD} distributions predicted by the Monte Carlo simulation. The τ decay mode results in the peak at $E_{HAD}=0$ for $D_S^\pm$ production while the extra photon from the $D_S^{*\pm}$ decay washes the peak out.

D. Other sources

Several other contributions to low-E_{HAD} two-muon states contribute at the sub-event level. These include $\mu^+\mu^-$ decays from neutral-current (NC) diffractively produced J/ψ, $\mu^+\mu^-$ decays from NC diffractively produced light vector mesons, CC diffractively produced π^+ in which the pion decays, π^+ from CC baryon resonance production followed by pion decay, and quasi-elastic CC scattering where pattern recognition errors split the outgoing muon track into two.

1. NC diffractive vector meson sources

Diffractive production of vector mesons is an important process in photoproduction experiments. A similar process is available in the weak sector with the substitution of a Z^0 for the photon (Fig. 8). Vector mesons which can decay to two muons include ρ^0, ω, ϕ, and J/ψ.

The VMD model is used to predict the expected number of vector mesons. Cross sections are normalized to the Fermilab E632 measurement of neutrino production of single $\rho^\pm$ [27] with the NC and CC cross sections related by Pumplin's procedure [29]. The J/ψ estimate is calculated in the $SU(4)$ flavor limit for comparison purposes.

Table II lists the number of vector meson events predicted to be observed in the NuTeV data. All sources except J/ψ production are expected to be small, with the suppression largely attributable to the very small $\mu^+\mu^-$ branching fractions for vector mesons. Section V B describes a measurement of the J/ψ signal from diffractive production.

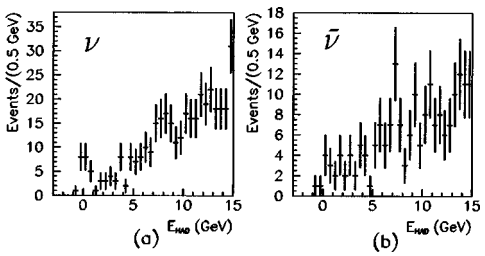

FIG. 11. The hadronic energy distribution for the two-muon data. The first 12 bins contribute to Figs. 13 and 14.

TABLE III. Predictions for the number of events expected to be observed by NuTeV in the low-E_{HAD} ($E_{HAD}<3$ GeV) two-muon sample.

	No. of events (ν)	No. of events ($\bar{\nu}$)	
DIS	10.4	4.0	Ref. [2]
Neutrino tridents	4.8	2.2	Refs. [9,10]
$D_S^{\pm}$	102.9	48.2	Refs. [7,8]
$D_S^{*\pm}$	33.0	13.6	Refs. [7,8]
Light vector mesons (ρ^0, ω, ϕ)	<0.12	<0.08	Refs. [27,29]
J/ψ (coherent)	4.88	1.86	Refs. [27,29]
J/ψ (incoherent)	17.1	7.76	Refs. [27,29]
Single $\pi^{\pm}$	<0.1	<0.1	Refs. [27,30]
$\Lambda_C^{\pm}$	<0.1	<0.1	Refs. [31]
Mis-identified single muon events	0.75	0.25	
Sum	174.4	78.2	

2. Sources from pion decay or misreconstruction

Single pions produced in NuTeV have two primary sources: diffractive and resonance production (Fig. 9). The density of the NuTeV detector limits the contribution of both sources to the two-muon sample since the pion must decay prior to interacting. Diffractive production is predicted using the PCAC model normalized to the measured cross section [27] resulting in 0.08 (0.02) estimated events in the ν ($\bar{\nu}$) mode. Resonance production can result in the decay of a final state pion with little visible hadronic energy. This is calculated with a model from Rein and Sehgal [30] and predicts <0.1 events in either mode.

Quasi-elastic production of $\Lambda_C^{\pm}$ events (Fig. 10) has also been considered [31]. The muon from the $\Lambda_C^{\pm}$ decay is of very low momentum, resulting in extremely low acceptance. We predict <0.1 events in either mode.

The final source considered was leakage from low-E_{HAD} single muon events due to misreconstruction. Contributions from this class of events were greatly reduced by requiring that the scintillator counters or drift chambers be consistent with two muons over a minimum length. The primary remaining source of these events was quasi-elastic scattering where multiple Coulomb scattering and drift chamber inefficiencies caused the pattern recognition software to find a spurious second track in the event. This contribution was estimated using straight-through muons which result from charged-current interactions upstream of the detector that enter the calorimeter. A random longitudinal event vertex was chosen, and all event information upstream of this point was discarded, leaving a topology identical to a quasi-elastic event. These straight-through muons were analyzed in the same way as the neutrino data sample and the results normalized to the observed number of single muon quasi-elastic events. The resulting predictions are 0.75 (0.25) events in the ν ($\bar{\nu}$) mode.

A summary of the predicted number of events from each source is shown in Table III. The remainder of this paper describes the measurement of the largest sources: DIS, neutrino tridents, $D_S^{\pm}/D_S^{*\pm}$, and J/ψ.

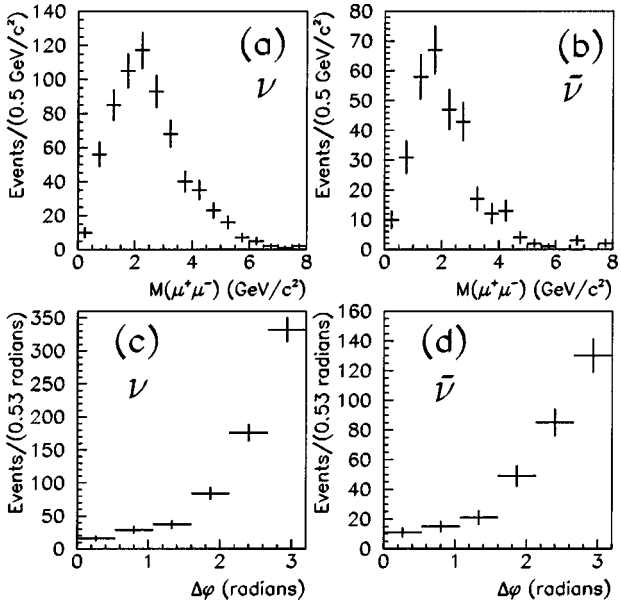

FIG. 12. Distributions for the two-muon NuTeV events with $E_{HAD}<15$ GeV. The plots are the two-muon invariant mass ($M_{\mu\mu}$) for ν (a) and $\bar{\nu}$ (b) modes and $\Delta\phi$ in ν (c) and $\bar{\nu}$ (d) modes.

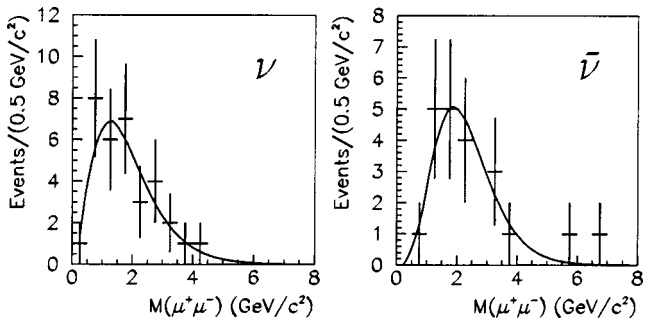

FIG. 13. The two-muon invariant mass ($M_{\mu\mu}$) for the low-E_{HAD} ($E_{HAD}<3$ GeV) two-muon data. The curve shows a fit to the distribution $x^{\alpha}e^{(\beta+\gamma x)}$.

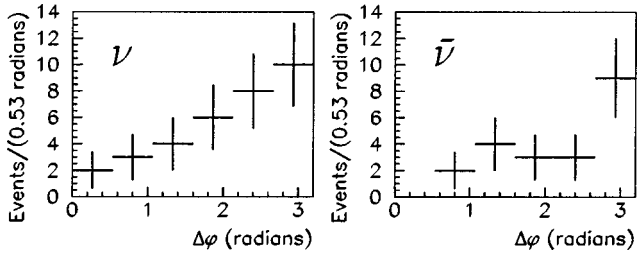

FIG. 14. The $\Delta\phi$ distributions for the low-E_{HAD} ($E_{HAD}<3$ GeV) two-muon data. $\Delta\phi$ is defined in the text.

V. RESULTS

A. Charged-current analysis

Our charged-current analysis examines three kinematic variables: the hadronic energy (E_{HAD}) up to 15 GeV, the two-muon invariant mass ($M_{\mu\mu}$), and the absolute value of the smallest difference between the muon azimuthal angles ($\Delta\phi$). Distributions for these quantities as measured in NuTeV data are shown in Figs. 11, 12, 13, and 14. Since the analysis is primarily concerned with events that peak at low E_{HAD}, the $M_{\mu\mu}$ (Fig. 13) and $\Delta\phi$ (Fig. 14) distributions are plotted with the additional restriction $E_{HAD}\leqslant 3$ GeV to emphasize the diffractive region. However, all events with $E_{HAD}\leqslant 15$ GeV are used in the subsequent fitting. Thirty-three neutrino and 21 anti-neutrino two-muon events were observed with $E_{HAD}<3$ GeV. These numbers are significantly below the sum of the predicted number of events in Table III, indicating that the naive $SU(4)$ flavor predictions for heavy quark final states are too large. On the other hand, there is a large excess over the predictions from DIS feed-down and neutrino trident production.

A fit was performed allowing up to four sources of low-E_{HAD} two-muon events: DIS, neutrino tridents, diffractive $D_S^{\pm}$, and diffractive $D_S^{*\pm}$. These sources were simulated via Monte Carlo calculations and normalized to the NuTeV inclusive two-muon samples. Figure 15 shows distributions of E_{HAD}, $M_{\mu\mu}$, and $\Delta\phi$ for the four major sources. Deep-inelastic scattering contributions peak at high $M_{\mu\mu}$ ($M_{\mu\mu}>2$ GeV/c^2), high E_{HAD}, and at $\Delta\phi=\pi$, the latter feature reflecting the essentially two-body final state of DIS charm production. The neutrino trident signal peaks at low E_{HAD}, low $M_{\mu\mu}$ and is more uniform in $\Delta\phi$. The D_S and D_S^* distributions are intermediate between DIS and neutrino tridents, with D_S distinguishable from D_S^* in the E_{HAD} distribution due to the decay photon contribution to E_{HAD} for D_S^*. Diffractive D_S and neutrino trident distributions are very similar; hence their measurements are highly correlated.

TABLE IV. Parameters from the three parameter fit to the low-E_{HAD} two-muon data.

Parameter	Result
DIS	$0.90^{+0.06}_{-0.06}$
Neutrino tridents	$0.72^{+1.20}_{-0.72}$
Diffractive charm ($D_S^{\pm}+D_S^{*\pm}$)	$0.18^{+0.05}_{-0.04}$

Data and Monte Carlo simulations were binned three dimensionally in (E_{HAD},$M_{\mu\mu}$,$\Delta\phi$) space: 18 bins in E_{HAD} ($-3-15$ GeV), 6 in $M_{\mu\mu}$ (0–6 GeV), and 6 in $|\Delta\phi|$ (0–π rad). The Monte Carlo is fit to the data using a maximum-likelihood technique. The Monte Carlo sets are summed together using a single normalization factor for each source which was defined to be 1.0 for the level presented in the preceding section. Neutrino and anti-neutrino modes were fit simultaneously.

The results of the fit are shown in Table IV. Figure 16 compares these results to the data and shows that we are able to describe the data with the four largest sources. The DIS contribution is consistent with that expected from the higher

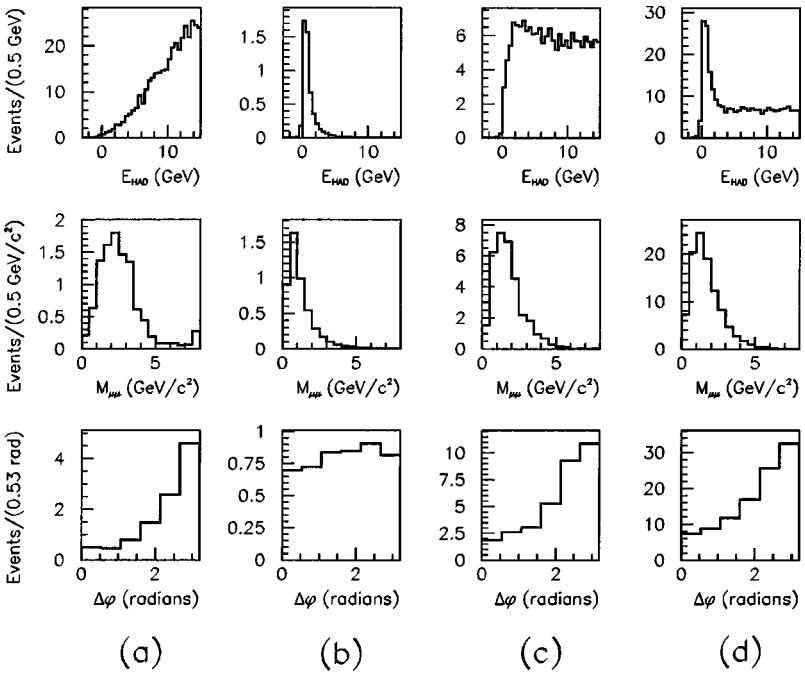

FIG. 15. Monte Carlo distributions of visible hadronic energy, two muon invariant mass and $\Delta\phi$ for the four largest sources of low-E_{HAD} two-muon events: (a) DIS charm, (b) neutrino tridents, (c) diffractive $D_S^{*\pm}$, (d) diffractive $D_S^{\pm}$. The invariant mass and $\Delta\phi$ distributions are for $E_{HAD}<3$ GeV.

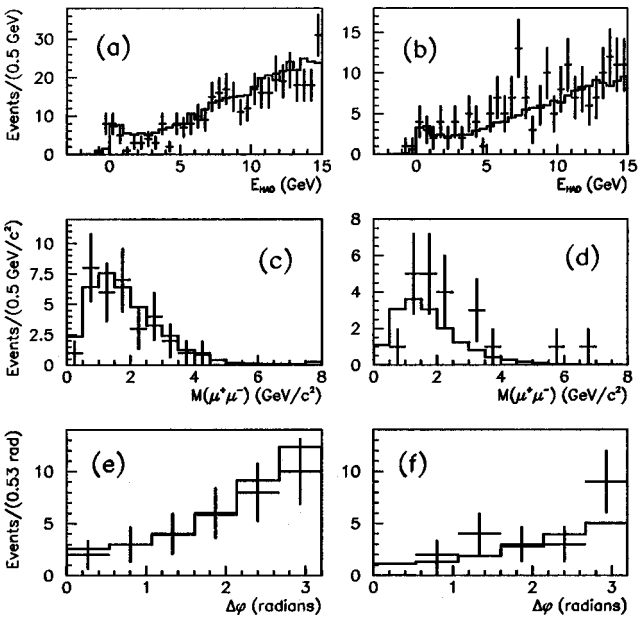

FIG. 16. Comparison of the final result (Monte Carlo simulation) to the low-E_{HAD} two-muon data for (a),(b) E_{HAD}, (c),(d) $M_{\mu^+\mu^-}$, (e),(f) $\Delta\phi$. The left side is the ν mode; the right side is the $\bar{\nu}$ mode. The $M_{\mu^+\mu^-}$ and $\Delta\phi$ distributions are for $E_{HAD}<3$ GeV. The points represent the data while the histogram shows the Monte Carlo simulation.

E_{HAD} two-muon analysis [2]. The neutrino trident contribution is consistent with the standard model prediction, but cannot distinguish between $V-A$ and the standard model. This is in contrast to a previous analysis which ruled out $V-A$ [21]. However, none of the previous analyses considered diffractive sources [21–23,26].

The consideration of all sources of low-E_{HAD} two-muon events allows us to measure diffractive charm production. The $D_S^{\pm}$ and $D_S^{*\pm}$ sources have been combined in proportion to the theoretical predictions and a single fit parameter used. This yields cross sections of

$$\sigma(\nu_\mu \mathrm{Fe}\to\mu^-(D_S+D_S^*)\mathrm{Fe})=(3.3\pm0.8)\ \ \text{fb/nucleon},$$

evaluated at $E_\nu=130$ GeV using the modified VMD and PCAC predictions to extrapolate in energy under the assumptions $\sigma(\nu_\mu \mathrm{Fe}\to\mu^- D_S^{*+}\mathrm{Fe})=\sigma(\bar{\nu}_\mu \mathrm{Fe}\to\mu^+ D_S^{*-}\mathrm{Fe})$ and $\sigma(\nu_\mu \mathrm{Fe}\to\mu^- D_S^{+}\mathrm{Fe})=\sigma(\bar{\nu}_\mu \mathrm{Fe}\to\mu^+ D_S^{-}\mathrm{Fe})$. A second fit performed with the neutrino trident parameter fixed to the standard model prediction yielded the consistent results $\sigma(\nu_\mu \mathrm{Fe}\to\mu^-(D_S+D_S^*)\mathrm{Fe})=(3.0\pm0.6)$ fb/nucleon at $E_\nu=130$ GeV.

Several systematic effects were considered. The hadronic energy measured by the calorimeter has been studied independently and shown to reconstruct energies down to the lowest available π^- beam at 5 GeV/c [14]. The Monte Carlo hadronic energy scale was varied by 5% which produced an error of less than 0.05 fb/nucleon in the cross section. The choice of binning was varied. Also, the hadronic energy was calculated over a fixed length (7 counters from the upstream end) rather than the variable length described in Sec. III. None of these had a significant effect on the result. The slope of the t distribution (b) was varied by 10% which resulted in very small changes in the event kinematics. Finally, this result assumes an isotropic D_S^* decay. Studies showed the effects of a possible D_S^* polarization to be small. The largest change, corresponding to nearly complete longitudinal polarization, lowered $\sigma(D_S+D_S^*)$ by 0.4 fb/nucleon. These studies confirmed that the result is completely dominated by the statistical error.

TABLE V. Measured event contributions to the low-E_{HAD} two-muon event sample.

	No. of events (ν)	No. of events ($\bar{\nu}$)
J/ψ (90% C.L.)	<7.5	<5.0
DIS	$9.4^{+0.6}_{-0.6}$	$3.6^{+0.3}_{-0.3}$
Neutrino tridents	$3.5^{+5.8}_{-3.5}$	$1.6^{+2.7}_{-1.6}$
$(D_S^{\pm}+D_S^{*\pm})$	$24.5^{+5.7}_{-5.8}$	$11.1^{+2.6}_{-2.6}$
Mis-identified single muon events	0.75 ± 0.43	0.25 ± 0.25
All other sources (estimate)	<0.1	<0.1

Previously, the Big Bubble Chamber Neutrino Collaboration combined various data samples to measure the diffractive rate of charmed strange mesons $(D_S^{\pm}+D_S^{*\pm})$ per charged-current νI (I is an isoscalar target) interaction [7]. They measured a rate of $(2.8\pm1.1)\times10^{-3}$. The observation of $D_S^{*\pm}$ production by CHORUS [8] is in agreement with this rate. Using the results of our second fit, we find a rate of $(3.2\pm0.6)\times10^{-3}$, which is consistent with previous results.

Table V lists the number of events contribution of each source in the low-E_{HAD} two muon data sample as determined by this analysis.

B. Neutral-current analysis

Neutral-current J/ψ production produces a clear signature in the two muon invariant mass, particularly if $E_{HAD}\leqslant3$ GeV is imposed to select diffractively produced events. There is no evidence for a J/ψ signal in Fig. 13; however, the relatively poor resolution of the NuTeV detector may be obscuring a contribution from this source. To assess this possibility, a diffractive J/ψ sample was simulated via Monte Carlo simulation to obtain the $M_{\mu\mu}$ distribution shown in Fig. 17. A Gaussian fit to this distribution yields a resolution $\sigma_0=0.40$ GeV/c^2.

A maximum likelihood fit was then performed to determine the amount of J/ψ present in the data. The fit function was taken to be

$$N(M_{\mu\mu})=M_{\mu\mu}^{\alpha}e^{(\beta+\gamma M_{\mu\mu})}+A\exp\left[-\frac{1}{2}\left(\frac{M_{\mu\mu}-M_0}{\sigma_0}\right)^2\right], \tag{5.1}$$

where $M_{\mu\mu}$ is the two muon invariant mass. M_0 and σ_0 are the mass and width of the J/ψ as measured by the Monte Carlo calculation. The first term represents a smooth parametrization of the background description where α and γ de-

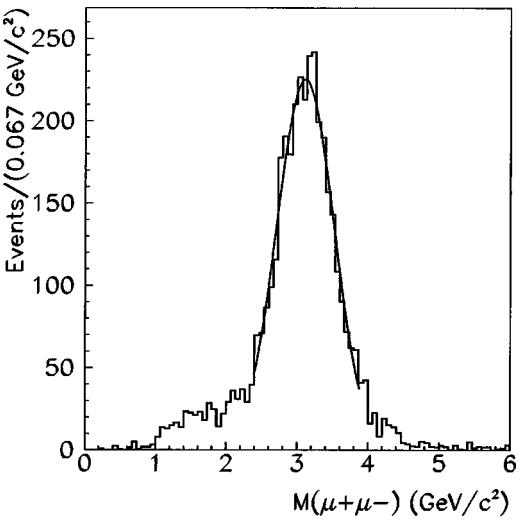

FIG. 17. The two muon invariant mass ($M_{\mu\mu}$) for the J/ψ Monte Carlo simulation. The distribution is unnormalized. The curve shows a Gaussian fit.

termine the shape and β the normalization. The second term is a Gaussian description of the J/ψ contribution with mean mass M_0 and width σ_0 set to the Monte Carlo prediction. The parameter A measures the amount of J/ψ in the data.

The results of the fit are shown in Table VI. A 90% confidence level (C.L.) on the J/ψ contribution is set by fixing the J/ψ amplitude to various increasing levels and fitting for the background. The likelihood function $[\mathcal{L}(A)]$ was plotted as a function of A and the 90% C.L. limit set by $\int_{A_0}^{A_{\rm C.L.}}\mathcal{L}(A)dA/\int_{A_0}^{\infty}\mathcal{L}(A)dA=0.90$. The resulting number of events is found by integrating the Gaussian with amplitude $A_{\rm C.L.}$ and converting to a cross section by normalizing to the DIS two-muon sample. The 90% confidence level limits on the diffractive J/ψ cross section are

$$\sigma(\nu_\mu \mathrm{Fe}\rightarrow \nu_\mu J/\psi \mathrm{Fe})\leqslant 0.21 \text{ fb/nucleon at } 90\% \text{ C.L.},$$

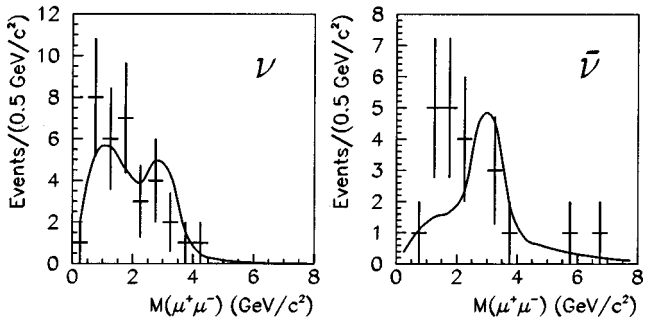

FIG. 18. The 90% confidence level limit on diffractive J/ψ production. The curve shows the fit to the background with the 90% C.L. contribution from J/ψ.

$$\sigma(\bar{\nu}_\mu \mathrm{Fe}\rightarrow \bar{\nu}_\mu J/\psi \mathrm{Fe})\leqslant 0.36 \text{ fb/nucleon at } 90\% \text{ C.L.},$$

at a mean production energy of $E_\nu=175$ GeV for $E_{HAD}\leqslant 3$ GeV. Figure 18 shows the results of this limit including the J/ψ contribution.

Using the VMD model, we can extrapolate the J/ψ cross section to lower E_ν to compare to the CDHS measurement of (0.042 ± 0.015) fb/nucleon. Figure 19 shows a 90% C.L. limit for the J/ψ cross section normalized to the NuTeV measurement and compares to the CDHS result. The energy behavior of this limit is dependent upon the model inputs. We show the limit for a momentum transfer squared (t) distribution of e^{-145t} [27] and coherent production only. The interpretation of the CDHS measurement as diffractive production is contradicted by our limit; however, the CDHS E_{HAD} cut of 10 GeV compared to a mean neutrino energy of 70 GeV could have accepted DIS production of J/ψ.

The analysis was repeated with a higher E_{HAD} cut ($E_{HAD}<10$ GeV) which matches the CDHS selection. The results are also included in Table VI. The limit as a function of E_ν is shown as the dashed curve in Fig. 19. While this limit is near the CDHS measurement, the diffractive J/ψ

TABLE VI. Limits on diffractive J/ψ production observed by NuTeV in the low-E_{HAD} two-muon sample.

	ν mode	$\bar{\nu}$ mode
$E_{HAD}<3$ GeV		
No. of events (fit)	3.3 ± 3.5	-1.7 ± 2.8
No. of events (90% C.L.)	7.5	5.0
Average E_ν (J/ψ) (GeV)	185.0	168.0
Cross section (90% C.L.) ($E_\nu=175$ GeV) (fb/nucleon)	0.19	0.32
Cross section (90% C.L.) ($E_\nu=70$ GeV)(fb/nucleon)	0.011	0.017
$E_{HAD}<10$ GeV		
No. of events (fit)	7.8 ± 10.1	-2.4 ± 7.4
No. of events (90% C.L.)	24.8	11.5
Cross section (90% C.L.) ($E_\nu=175$ GeV) (fb/nucleon)	0.63	0.73
Cross section (90% C.L.) ($E_\nu=70$ GeV) (fb/nucleon)	0.034	0.040
CDHS result ($E_{HAD}<10$ GeV)		
Cross section (fit) ($E_\nu=70$ GeV)(fb/nucleon)	(0.042 ± 0.015)	

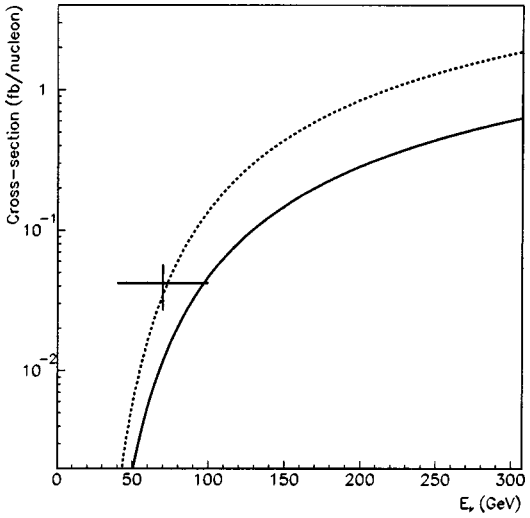

FIG. 19. Energy dependence of the 90% confidence level limit on diffractive J/ψ production normalized to the NuTeV measurement. The solid line is the limit set with $E_{HAD}<3$ GeV and the dashed line with $E_{HAD}<10$ GeV. The data point shows the CDHS measurement.

Monte Carlo calculation shows that the lower E_{HAD} (<3 GeV) is appropriate for coherent diffractive production. One possible explanation is that the higher cut allows a contribution from DIS J/ψ production.

For completeness, the E_{HAD} cut was changed to $E_{HAD}>10$ GeV to allow a search for inclusive DIS J/ψ production. Figure 20 shows the resulting $M_{\mu\mu}$ distribution. A fit was performed with the background modelled by an asymmetric Gaussian function and the data binned in 0.5 GeV/c^2 intervals. No statistically significant J/ψ signal was found, and 90% confidence level limits for the (DISJ/ψ)/(DIS CC charm) rates were found to be

$$\frac{N(\nu_\mu N\to\nu_\mu J/\psi X)}{N(\nu_\mu N\to\mu^- cX)}\leqslant 0.024 \text{ at } 90\% \text{ C.L.},$$

$$\frac{N(\bar{\nu}_\mu N\to\bar{\nu}_\mu J/\psi X)}{N(\bar{\nu}_\mu N\to\mu^+\bar{c}X)}\leqslant 0.069 \text{ at } 90\% \text{ C.L.},$$

when averaged over the NuTeV beam spectra. Assuming a similar energy dependence to DIS CC charm production, this corresponds to cross-section limits evaluated at $E_\nu=125$ GeV,

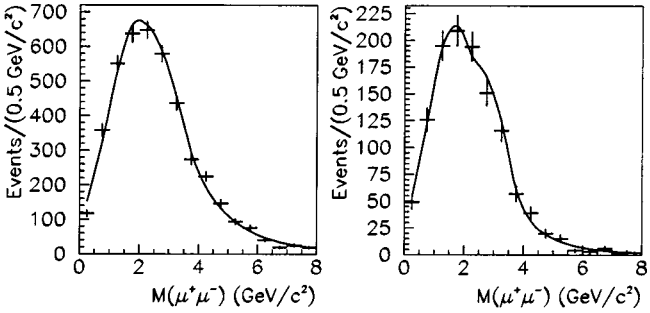

FIG. 20. The two muon invariant mass distribution for high E_{HAD} ($E_{HAD}>10$ GeV). The curve shows the fit to the background with the 90% C.L. contribution from J/ψ.

$$\sigma(\nu_\mu N\to\nu_\mu J/\psi X)\leqslant 2.2 \text{ fb/nucleon at } 90\% \text{ C.L.},$$

$$\sigma(\bar{\nu}_\mu N\to\bar{\nu}_\mu J/\psi X)\leqslant 3.4 \text{ fb/nucleon at } 90\% \text{ C.L.},$$

at an average DIS CC charm production energy of $E_\nu=125$ GeV. Figure 20 shows the 90% C.L. curve for the inclusive ($E_{HAD}>10$ GeV) DIS two-muon sample.

VI. CONCLUSIONS

We have performed an inclusive analysis of the low-E_{HAD} two-muon data sample available from NuTeV. All known standard model processes have been considered, and four significant sources were found to contribute: DIS, neutrino trident, diffractive $D_S^\pm$, and diffractive $D_S^{*\pm}$. We have measured diffractive $D_S^\pm$ and $D_S^{*\pm}$ cross sections to be 1.4 ± 0.3 fb/nucleon and 1.6 ± 0.4 fb/nucleon, respectively, for ν_μFe scattering at $E_\nu=130$ GeV, in agreement with previous results assuming a VMD energy dependence of the cross section. The data are consistent with neutrino trident production from standard model predictions. Finally, we see no evidence for either diffractive or DIS production of J/ψ in NC ν_μ and $\bar{\nu}_\mu$ scattering on iron.

ACKNOWLEDGMENTS

We would like to thank the staffs of the Fermilab Particle Physics and Beams Divisions for their contributions to the construction and operation of the NuTeV beamlines. We would also like to thank the staffs of our home institutions for their help throughout the running and analysis of NuTeV. This work has been sponsored by the U.S. Department of Energy and the National Science Foundation.

[1] J. Conrad, M. Shaevitz, and T. Bolton, Rev. Mod. Phys. **70**, 1341 (1998).
[2] T. Adams *et al.*, in Proceedings of the 33rd Rencontres de Moriond, QCD and Hadronic Interactions.
[3] P. Vilain *et al.*, Eur. Phys. J. C **11**, 19 (1999).
[4] A. O. Bazarko *et al.*, Z. Phys. C **65**, 189 (1995).
[5] S. A. Rabinowitz *et al.*, Phys. Rev. Lett. **70**, 134 (1993).
[6] H. Abramowicz *et al.*, Z. Phys. C **15**, 19 (1982).
[7] A. E. Asratyan *et al.*, Z. Phys. C **58**, 55 (1993).
[8] P. Annis *et al.*, Phys. Lett. B **435**, 458 (1998).
[9] R. Belusevic and J. Smith, Phys. Rev. D **37**, 2419 (1987).
[10] C. H. Llewellyn Smith, Phys. Rep. **3**, 261 (1972).
[11] H. Abramowicz *et al.*, Phys. Lett. **109B**, 115 (1982).
[12] W. S. Sakumoto *et al.*, Nucl. Instrum. Methods Phys. Res. A **294**, 179 (1991); B. J. King *et al.*, *ibid.* **302**, 254 (1991).
[13] NuTeV Collaboration, R. H. Bernstein *et al.*, ''Technical

Memorandum: Sign Selected Quadrupole Train,'' Report No. FERMILAB-TM-1884, 1994; NuTeV Collaboration, J. Yu *et al.*, ''Technical Memorandum: NuTeV SSQT performance,'' Report No. FERMILAB-TM-2040, 1998.
[14] D. Harris *et al.*, hep-ex/9908056.
[15] P. Collins and T. Spiller, J. Phys. G **11**, 1289 (1985).
[16] N. Ushida *et al.*, Phys. Lett. B **206**, 375 (1988).
[17] T. Bolton, hep-ex/9708014.
[18] Particle Data Group, C. Caso *et al.*, Eur. Phys. J. C **3**, 1 (1998).
[19] P. H. Sandler, Ph.D. thesis, University of Wisconsin-Madison, 1992.
[20] R. W. Brown *et al.*, Phys. Rev. D **6**, 3273 (1972).
[21] S. R. Mishra *et al.*, Phys. Rev. Lett. **66**, 3117 (1991).
[22] G. Geiregat *et al.*, Phys. Lett. B **245**, 271 (1990).
[23] F. Bergsma *et al.*, Phys. Lett. **122B**, 185 (1983).
[24] K. Fujikawa, Ann. Phys. (N.Y.) **68**, 102 (1971); **75**, 491 (1973).
[25] K. Fujikawa, Phys. Rev. D **8**, 1623 (1973).
[26] T. Adams *et al.*, in Proceedings of the 29th International Conference on High Energy Physics, Vancouver, Canada, 1998, edited by Alan Astbury, David Axen, and Jacob Robinson, p. 631.
[27] S. Willocq *et al.*, Phys. Rev. D **47**, 2661 (1993).
[28] B. Z. Kopeliovich and P. Marage, Int. J. Mod. Phys. A **8**, 1513 (1993).
[29] J. Pumplin, Phys. Rev. Lett. **64**, 2751 (1990).
[30] D. Rein and L. M. Sehgal, Ann. Phys. (N.Y.) **133**, 79 (1981).
[31] R. E. Shrock and B. W. Lee, Phys. Rev. D **13**, 2539 (1976); **14**, 313(E) (1976).